Designing of CHK1 inhibitors by 3D-QSAR, virtual screening and induced fit docking studies

Sayalee Chavan[1,*], Rajkumar Hirwani[1], M. Sarwar Alam[2], Nikhil Vidyasagar[1], Radhacharan Dash[1] and Veena Deshpande[1]

[1]CSIR Unit for Research and Development of Information Products, 'Tapovan', NCL Campus, S. No. 113, 114, Pashan, Pune 411 008, India
[2]Department of Chemistry, Faculty of Science, Jamia Hamdard, Hamdard Nagar, New Delhi 110 062, India

Checkpoint kinase 1 (CHK1) is an attractive therapeutic target for cancer treatment as CHK1 is a key mediator in the DNA damage-induced checkpoint network. The structure-based drug design approach was used to achieve this objective which includes the 3D-QSAR studies, where a series of selenophene derivatives to investigate the structural requirements of their inhibitory activity against CHK1 was used for the development of the model. The generated model was precise with $r^2 = 0.95$ and $q^2 = 0.68$. Furthermore, the study involves the use of structure-based virtual screening of specs database and induced fit docking studies to retrieve potential CHK1 inhibitors.

Keywords: Checkpoint kinase 1, induced fit docking, virtual screening, toxicity prediction.

CHECKPOINT kinase 1 (CHK1), belonging to the serine/threonine protein kinase family, is involved in cell cycle control[1]. CHK1 has an N-terminal kinase domain, a linker region, a regulatory SQ/TQ domain and a C-terminal domain[2,3].

CHK1 forms a core component of the DNA damage response[4]. In eukaryotic cells, genotoxic stress that damages the DNA or inhibits DNA synthesis causes activation of checkpoints[5], which leads to diverse cellular responses such as cell cycle arrest, DNA repair and cell death[6]. CHK1 has multiple roles in protecting cells from DNA damage, which may be a consequence of the cancer itself or caused by cancer treatments like chemotherapy. Inhibition of CHK1 affects the ability of the cell to repair this damage and can therefore potentiate the effect of certain chemotherapeutic drugs. CHK1 prevents premature entry into mitosis[7]. However, it is also involved in the stabilization of stalled replication forks[8], inhibition of origin firing and control replication fork progression[9], and homologous recombination[10]. Inhibition of CHK1 blocks the proliferation of cancer cell lines[11,12]. A recent study has shown that inhibition of CHK1 signalling is potential therapy in neuroblastoma.

CHK1 inhibitors have been explored as chemopotentiating agents since the discovery of UCN-01 (PDF) and several small molecule inhibitors of CHK1 are currently in early stage clinical trials[13].

AZD7762 (Astra Zeneca) is a selective CHK1 inhibitor, presently undergoing phase 1 clinical trial that increases the toxicity of DNA-damaging agents resulting in improved antitumour activity[14]. Similarly, SCH 900776 (Schering Plough) is a functionally selective inhibitor targeting cell-cycle-checkpoint kinase 1. LY2606368 (Eli Lily) and PF-477736 (Pfizer) are potent inhibitors of CHK1 that are currently undergoing phase-1 clinical trial[15,16].

Abrogation of camptothecin- or 5-fluorouracil-induced S-phase arrest or doxorubicin-induced G (2)-phase arrest has been noticed by down-regulation of CHK1 (ref. 1). From the literature it can be seen that CHK1 is the relevant checkpoint kinase as a cancer drug target. With these considerations we have performed a computational study to design potent and safe inhibitors of CHK1 using various *in silico* methods like three-dimensional structure activity relationships (3D-QSAR), induced field docking and virtual screening.

Material and methods

Dataset

A dataset comprising 31 compounds of selenophene derivatives reported as CHK1 inhibitors was selected for the present study[17]. The reported IC_{50} values of these derivatives were used to develop the 3D-QSAR model. Table 1 lists all the derivatives along with the experimental and predicted 1/log IC_{50} values.

3D-QSAR model generation

To identify the structural features required for the inhibitory activity, 3D-QSAR models were generated using

*For correspondence. (e-mail: sayalee@urdip.res.in)

Table 1. Dataset with experimental and predicted activities

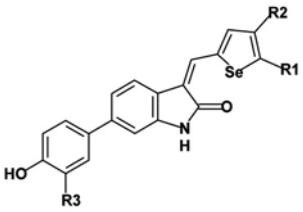

A

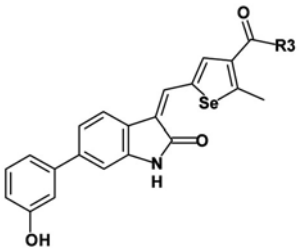

B

Core	No.	R1	R2	R3	Experiment pIC50 (nM)	Predicted pIC50 (nM)
A	1	H	H	OCH_3	0.232	0.228856
A	2	CH_3	H	OCH_3	0.242	0.232543
A	3	COOH	H	OCH_3	0.206	0.214278
A	4	CH_3	–COOH	OCH_3	0.245	0.235539
A	5	H	H	H	0.293	0.267497
A	6	CH_3	H	H	0.25	0.24886
A	7	CH_3	–COOH	H	0.274	0.266767
B	8	$CONH(CH_2)_2N(CH_3)_2$	H	OCH_3	0.254	0.250528
B	9	$CONH(CH_2)_2N(CH_2CH_3)_2$	H	OCH_3	0.28	0.271688
B	10	$CONH(CH_2)_2N(CH_2CH_2)_2$	H	OCH_3	0.371	0.37012
B	11	$CONH(CH_2)_2N(CH_2CH_2)_2O$	H	OCH_3	0.36	0.33974
A	12	$CONH(CH_2)_3$-1H-Imidazole	H	OCH_3	0.404	0.3785
A	13	CH_3	$CONH(CH_2)_2N(CH_3)_2$	OCH_3	0.333	0.346141
A	14	CH_3	$CONH(CH_2)_2N(CH_2CH_3)_2$	OCH_3	0.371	0.386741
A	15	CH_3	$CONH(CH_2)_2N(CH_2CH_2)_2$	OCH_3	0.243	0.260786
A	16	CH_3	$CONH(CH_2)_2N(CH_2CH_2)_2O$	OCH_3	0.234	0.227817
A	17	CH_3	$CONH(CH_2)_3$-1H-Imidazole	OCH_3	0.239	0.256692
A	18	$CONH(CH_2)_2N(CH_3)_2$	H	H	0.258	0.274129
A	19	$CONH(CH_2)_2N(CH_2CH_3)_2$	H	H	0.273	0.283083
A	20	$CONH(CH_2)_2N(CH_2CH_2)_2$	H	H	0.265	0.276667
A	21	$CONH(CH_2)_2N(CH_2CH_2)_2O$	H	H	0.274	0.275682
A	22	$CONH(CH_2)_3$-1H-Imidazole	H	H	0.256	0.305135
A	23	CH_3	$CONH(CH_2)_2N(CH_3)_2$	H	0.36	0.368944
A	24	CH_3	$CONH(CH_2)_2N(CH_2CH_3)_2$	H	0.384	0.360451
A	25	CH_3	$CONH(CH_2)_2N(CH_2CH_2)_2$	H	0.384	0.391974
A	26	CH_3	$CONH(CH_2)_2N(CH_2CH_2)_2O$	H	0.344	0.286137
A	27	CH_3	$CONH(CH_2)_3$-1H-Imidazole	H	0.371	0.339704
B	28	–	–	$NH(CH_2)_2N(CH_3)_2$	0.221	0.211266
B	29	–	–	$NH(CH_2)_2N(CH_2CH_3)_2$	0.204	0.222524
B	30	–	–	$NH(CH_2)_2N(CH_2CH_2)_2$	0.205	0.208713
B	31	–	–	$NH(CH_2)_3$-1H-Imidazole	0.208	0.223559

**t*, Test set compounds.

Phase module (Small-Molecule Drug Discovery Suite 2013-3: Phase, version 3.7, Schrödinger, LLC, New York, NY, 2013). Atom-based 3D-QSAR generation tool was used, as the selected dataset has similar structural framework. Atom-based alignment technique is good for the dataset having some common structural features among the molecules. A 3D structure of each molecule was built and all the molecules were minimized using the default universal force field within Maestro. A maximum of 2500 conformers were generated per structure using minimization of 100 steps. Combinations of Monte-Carlo Multiple Minimum (MCMM) and LowMode (LMOD) were used to study the conformational space of all the molecules[18]. Each minimized conformer was filtered through a relative energy gap of 10 kJ mol^{-1} and a minimum atom deviation of 2.00 Å. The whole dataset of selenophene derivatives was divided into training and test sets in a random manner. The best 3D-QSAR model was validated by predicting activities for the test set of six molecules using third partial least squares (PLS) factor. Figure 1 depicts the correlation graph between predicted and actual 1/log IC_{50} for both training and test sets.

Protein preparation

The crystal structure of protein CHK1 was obtained from Protein Data Bank [PDB ID: 2YEX]. The protein was

prepared using Protein Preparation Wizard (Schrödinger Suite 2013 Protein Preparation Wizard; Epik version 2.6, Schrödinger, LLC, New York, NY, 2013; Impact version 6.1, Schrödinger, LLC, New York, NY, 2013; Prime version 3.4, Schrödinger, LLC, New York, NY, 2013). In the protein preparation process, water molecules were removed, hydrogen atoms were added and bond orders were assigned. Further, a grid at the active site of the prepared protein structure was developed for docking. The grid spacing was kept at 20 Å.

Molecular docking

To investigate the detailed intermolecular interactions between the ligand and the target enzyme/protein, an automated docking program Glide was used. Three-dimensional crystal structure of target protein (PDB ID 2YEX) available in the protein Data Bank was used for docking. Prepared active molecules among selenophene derivatives were subjected to standard precision (SP) docking followed by extra precision (XP) docking using Glide module of Schrödinger suit (Small-Molecule Drug Discovery Suite 2013-3: Glide, version 6.1, Schrödinger, LLC, New York, NY, 2013). In XP docking 5 poses per ligand were generated with 1000 poses per docking run with an RMSD deviation of less than 0.5 Å.

Virtual screening

To identify potent CHK1 inhibitors, structure-based virtual screening was performed. Specs database was screened using Schrödinger's virtual screening protocol. Grid of the CHK1 protein (PDB ID 2YEX) was prepared and used for screening. The process of screening was started with the high throughput virtual screening (HTVS) method (Small-Molecule Drug Discovery Suite 2013-3: Glide, version 6.1, Schrödinger, LLC, New York, NY, 2013) followed by SP docking and XP docking with 10% cut-off at each step.

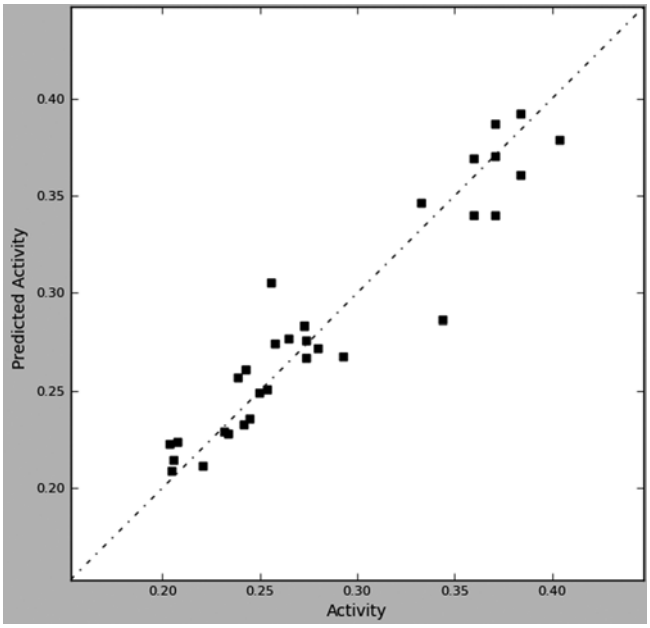

Figure 1. Experimental versus predicted 1/log IC_{50} of training and test sets.

Induced field docking

The process for the induced fit docking protocol developed by Schrödinger (Induced Fit Docking protocol 2013-3, Glide version 6.1, Prime version 3.4, Schrödinger, LLC, New York, NY, 2013) includes the importation of the receptor ligand complex into the workspace[19,20]. The complex is split into the ligand and water. The ligand was specified to be docked into the receptor. The receptor centroid core was picked up to generate the box for defining the core. Then the initial glide docking options, prime energy refinement as well as final glide re-docking parameters were specified to initiate the induced fit docking protocol.

In silico toxicity prediction

In order to discard undesirable hits in early stages of drug discovery, *in silico* toxicity prediction of both the hits was performed. DEREK Nexus version 4.1.0, Nexus: 2.0.0 from Lhasa limited was used for toxicity prediction[21]. DEREK is a knowledge-based expert system which helps predict the potential toxicity caused by a chemical by assessment of its structure. The qualitative predictions made by DEREK are based upon the structural alerts and rules contained in the DEREK knowledge base. The query structure is imported in SD file format/Molfile format. For toxicity prediction, first the structural features in the query structure are matched with the toxicophores (alerts) present in the knowledge base. The reasoning system then determines the likelihood of a structure being toxic, which is expressed as the likelihood levels. The prediction is done for a broad range of toxicological end-points for all the species.

Results and discussion

3D-QSAR model generation

The aim of this study was to elucidate and quantify the structural features of *N*-iso-propyl pyrrole-based derivatives crucial for binding, by generating atom based 3D-QSAR model. Phase module of Schrödinger suite was used to build 3D-QSAR model. Table 2 provides the details. For generating an atom-based 3D-QSAR hypothesis,

we have used a dataset of 25 (training set) compounds having inhibitory activity against CHK1. The model was validated using six (test set) compounds, which cover a wide range of CHK1 inhibitory activity. The PHASE descriptors served as independent variables and activity values as dependent variables in deducing 3D-QSAR models by the partial least square (PLS) regression analysis method. Statistical parameters were used for the test set predictions. The large value of $F = 153.5$, $r^2 = 0.9564$ indicates a statistically significant regression model, which is also supported by the small value of the variance ratio $P = 1.93e\text{-}014$, and SD = 0.014 as the indicator of a high degree of confidence. The test set had highest value of $q^2 = 0.681$, Pearson-$R = 0.8507$ and lowest value of RMSE = 0.04.

3D-QSAR interpretation

3D-QSAR models were interpreted by contribution maps (Figure 2). Blue and red cube areas indicate favourable and unfavourable regions respectively, to show activity of the molecule. The contribution map of H-bond donor (Figure 2 *a*) shows blue cube area at para position of phenyl ring indicating presence of H-bond donor group at that position, which increases the biological activity. It explains the activity of compounds 1–27 in which presence of hydroxyl group at para position of phenyl ring acts as H-bond donor which increases the biological activity. In contrast, in compounds 28–31, the hydroxyl group is present at meta position instead of para position, which decreases the biological activity. Presence of amide group attached to the selenophene ring has favourable effect on the biological activity, which explains the activity of compounds 8–31. Nitrogen of pyrolidine ring acts as a H-bond donor which is favourable for activity, which in turn explains the activity of compounds 25 and 26.

In hydrophobic contribution map (Figure 2 *b*) blue cube area near meta position of phenyl ring shows that presence of bulky group at that position increases the activity as in compounds 1–4 and 8–17. Blue cube area in the vicinity of the selenophene ring shows that bulky groups attached to 2-methyl selenophene-3-carboxamido ring increase the biological activity. This phenomenon is seen in the compounds 13–17. However, absence of aromatic or bulky groups at the third position of selanophene ring has a negative effect on biological activity, as seen in compounds 18–22. Presence of tertiary nitrogen group attached to 2-methyl selenophene-3-carboxamido ring has favourable effect on biological activity as seen in compounds 23–26.

In electron withdrawing contribution map (Figure 2 *c*), blue cube area near para position of phenyl ring indicates that presence of electron withdrawing group at para position of phenyl ring has favourable effect on biological activity. In contrast, red cube area in the vicinity of meta position of phenyl ring shows that presence of electron withdrawing group at meta position of phenyl ring decreases the biological activity. This phenomenon is seen in compounds 28–31, in which hydroxyl group is present at meta position. In compounds 1–4 and 8–17, presence of methoxy group at meta position has negative effect on biological activity. Blue cube area close to the third position of selenophene ring shows that presence of electron withdrawing group at that position increases the biological activity. It explains the behaviour of compounds 3, 4 and 7 in which presence of carboxyl group increases the biological activity and likewise, the presence of amide group at that position increases the biological activity.

In the electronegative contribution map (Figure 2 *d*), red cube area near the second and third positions of selenophene ring indicates that presence of electro-negative group at these positions decreases the biological activity as shown in the compounds 3, 4 and 7, where presence of carboxyl group has negative effect on biology.

In electro-positive contribution map (Figure 2 *e*), blue cube area near the third position of the selenophene ring shows that presence of electro-positive group at that position has favourable effect on biological activity. This can be seen in compounds 13–16 and 23–26, in which presence of quaternary nitrogen increases the biological activity.

Table 2. Statistical values for 3D-QSAR model generated by PLS

Training set	Test set
$m = 6$	
$n = 25$	$n_T = 6$
$r^2 = 0.9564$	$q^2 = 0.681$
SD = 0.014	RMSE = 0.04
$F = 153.5$, $P = 1.93e\text{-}014$	Pearson-$R = 0.8507$

m, Number of PLS factors in the model; *n*, Number of molecules in the training set; n_T, Number of molecules in the test set; r^2, Coefficient of determination; $q^2 = r^2$ for test set; SD, Standard deviation of regression; RMSE, Root mean square error; *F*, Variance ratio; *P*, Statistical significance; Pearson-*R*, Pearson correlation coefficient.

Molecular docking

The 3D-QSAR model was validated by docking study. Glide module of Schrödinger was used to evaluate the binding interactions of active ligands with the crystal structure of CHK1 protein (PDBID: 2YEX) present in the protein Data Bank.

Figure 3 shows the binding interactions of one of the active compounds (2) with crystal structure of CHK1 protein. It can seen that phenolic OH group acts as a H-bond donor and forms a H-bond with GLU55 with bond distance 1.74 Å, this supports the 3D-QSAR model, and shows H-bond donor at that particular position increases the biological activity. The secondary nitrogen of indole

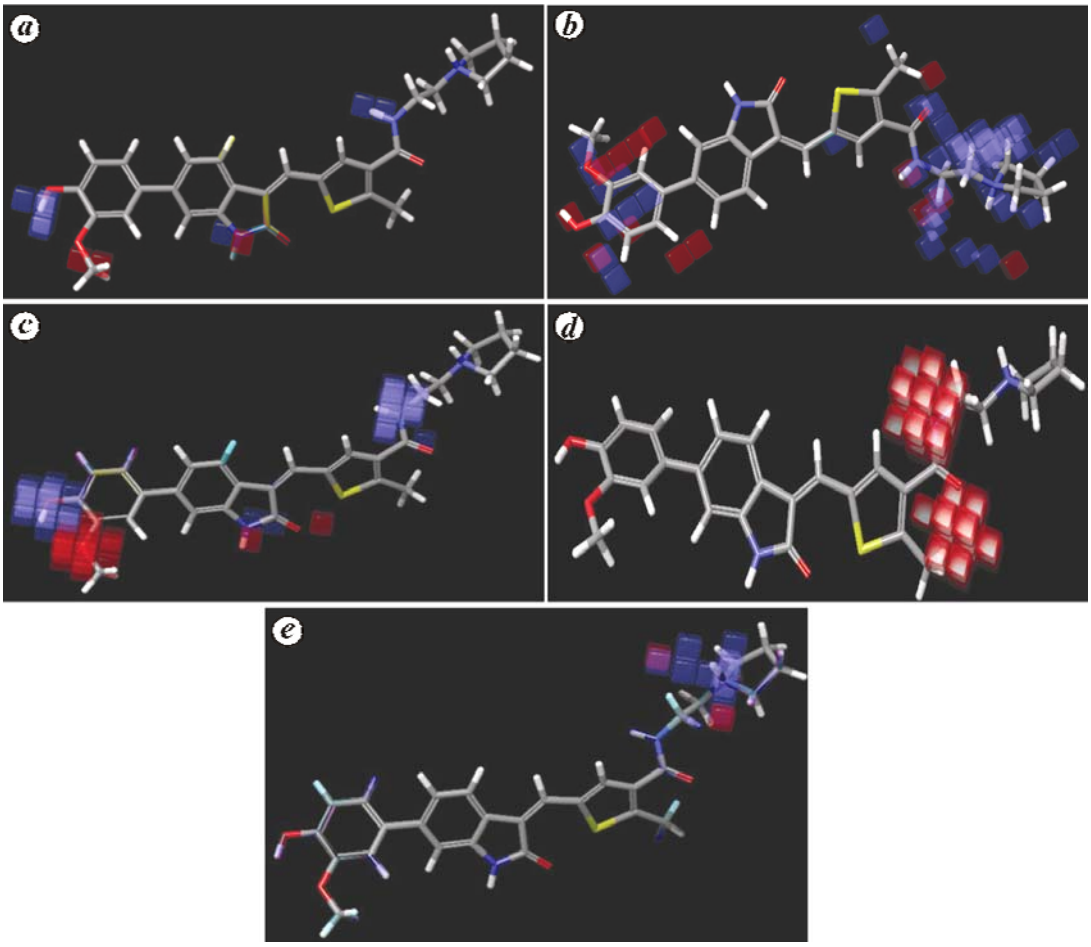

Figure 2. 3D-QSAR visualization for compound no. 12; (***a***) H-bond donor effect; (***b***) hydrophobic effect; (***c***) electron-withdrawing group effect; (***d***) electron-negative group effect; (***e***) electron-positive group effect.

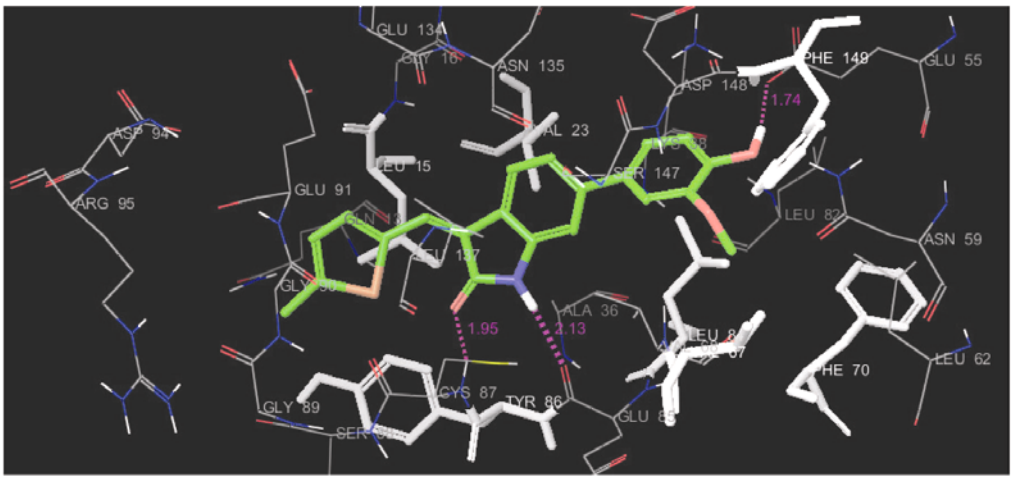

Figure 3. Docking interaction of compound 2 with CHK1 (PDB ID: 2YEX; white bond in tube, Hydrophobic interactions; dotted bond, H-bond formation).

ring acts as a H-bond donor and forms H-bond with GLU85 with bond distance 2.1 Å, present in an active site of CHK1 protein. The carbonyl oxygen of indole ring acts as a H-bond accepter and forms a H-bond with CYS87 residue with bond distance 1.95 Å. The hydrophobic chain of the inhibitors interacts with aromatic residues of

PHE70, TYR86 and PHE149. All these interactions highlight the good complementarity between the proposed 3D-QSAR models.

High-throughput virtual screening

Virtual screening is a cheap and fast method to identify potent drug candidates from a library of compounds. Based on the active site of CHK1 (PDB ID 2YEX), high throughput virtual screening was performed using the Specs database containing about 300,000 compounds. Glide module (Schrödinger suite 2011) was used for screening, which has three steps of docking protocol, namely HTVS, standard precision (SP) and extra precision (XP). In the first step, HTVS screens the compounds and passes them to the SP docking step. HTVS and SP modes are used for large sets of ligands and XP docking uses the top-ranked compounds from SP docking. Top 10% molecules from SP docking are then subjected to more accurate XP docking. From this protocol two hits were retrieved (Figure 4) having docking score ≥ 10. XP visualizer was used to analyse the binding interactions of hits with the CHK1 protein (PDB ID 2YEX). Figure 5 shows the binding interactions of one of the hits with the CHK1 protein.

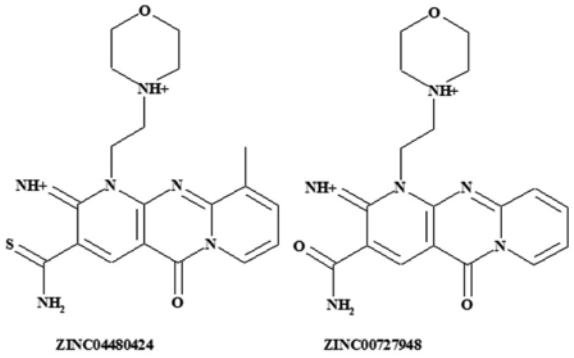

Figure 4. Final two screened hits.

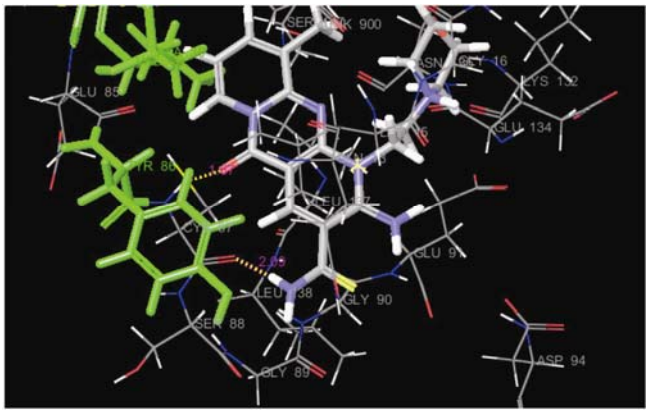

Figure 5. Binding conformation of hit ZINC04480424 with CHK1. (Green bond in tube, Hydrophobic interactions; dotted bond: H-bond formation.)

Induced fit docking

The induced fit docking module developed by Schrödinger was used to perform docking studies. It uses the docking module Glide to analyse ligand flexibility and the refinement module in Prime for analysis of receptor flexibility. Induced fit docking mode generates different receptor structures which are able to accommodate different ligand structures.

The procedure has an initial softened-potential; docking into a rigid receptor to generate an ensemble of poses; sampling of the protein for each ligand pose is generated in the first step; this is followed by redocking of the ligand into low-energy induced-fit structures from the previous step; scoring is done by accounting for the docking energy (Glide score), and receptor strain solvation terms (Prime energy).

Ligand code ZINC00727948 shows good binding interactions (Figure 6 *a*) with GLU 85, 91, 135 and CYS 87, and IFD score of 608.013, prime energy of 11931.4 and g score of 11.442 (Table 3).

Ligand code ZINC04480424 shows good binding interactions (Figure 6 *b*) with GLU 17, CYS 87 and GLU 91, and IFD score of 609.056, prime energy of 11,940.2 and g score –12.044 (Table 3).

In-silico toxicity prediction

To evaluate safety of retrieved hits, both hits were run in DEREK software for toxicity prediction. The structural

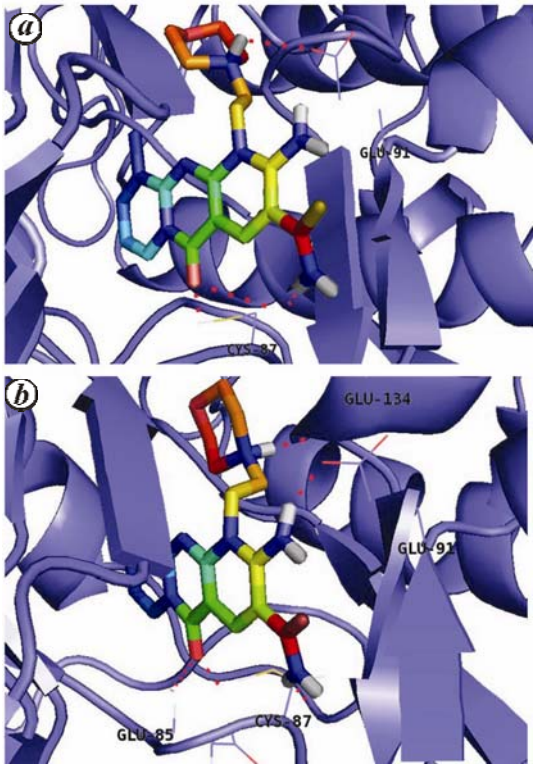

Figure 6. Induced fit docking interactions. ***a***, Hit ZINC00727948 with CHK1. ***b***, ZINC04480424 with CHK1.

Table 3. Induced fit docking scores of retrieved hits

Complex	Docking score	Glide g score	Glide emodel	Prime Energy	IFD_Score	Interactions
2YEX_948	–11.442	–11.442	–126.816	–11931.4	–608.013	GLU 85, 91, 134 CYS 87
2YEX_424	–12.044	–12.044	–163.140	–11940.2	–609.056	GLU 17, CYS 87 GLU 91

features in both the query structures do not match any of the toxicophores present in the knowledge base, so no structural alerts were received from DEREK. Thus, the results suggest that both the molecules do not have the potential for toxicity.

Conclusions

The present study elucidates key structural requirements for the inhibitory activity against CHK1 utilizing 3D-QSAR model. This model was prepared from a series of selenophene derivatives with known CHK1 inhibitory activity. The developed 3D-QSAR model is statistically significant and provides information about various favourable and unfavourable structural features responsible for inhibitory activity. Docking study was performed to evaluate the generated 3D-QSAR model. It has been found that the results of the docking correlate with the 3D-QSAR model. Two novel hits were retrieved by structure-based virtual screening of specs database. *In silico* toxicity studies showed that retrieved hits were non-toxic. The induced-fit docking studies reveal the exact conformational pose of the hits into the binding site of the target protein with H-bond interactions. These *in silico* evaluations will be beneficial to prioritize the experimental protocols and considerably reduce the time taken for drug discovery process.

1. Xiao, Z., Xue, J., Sowin, T. J. and Zhang, H., Differential roles of checkpoint kinase 1, checkpoint kinase 2, and mitogen-activated protein kinase-activated protein kinase 2 in mediating DNA damage-induced cell cycle arrest: implications for cancer therapy. *Mol. Cancer Ther.*, 2006, **8**, 1935–1943.
2. Sanchez, Y., Wong, C., Thoma, R. S., Richman, R., Wu, Z., Piwnica-Worms, H. and Elledge, S. J., Conservation of the Chk1 checkpoint pathway in mammals: linkage of DNA damage to Cdk regulation through Cdc25. *Science*, 1997, **277**, 1497–1501.
3. Chen, P. *et al.*, The 1.7 Å crystal structure of human cell cycle checkpoint kinase Chk 1: implications for Chk1 regulation. *Cell*, 2000, **100**, 681–692.
4. Bryant, C., Scriven, K. and Massey, A. Inhibition of the checkpoint kinase Chk1 induces DNA damage and cell death in human leukemia and lymphoma cells. *Mol. Cancer*, 2014, **13**, 147.
5. Hartwell, L. H. and Weinert, T. A., Checkpoints: controls that ensure the order of cell cycle events. *Science*, 1989, **246**, 629–634.
6. Zhou, B. B. and Elledge, S. J., The DNA damage response: putting checkpoints in perspective. *Nature*, 2000, **408**, 433–439.
7. McNeely, S. *et al.*, Chk1 inhibition after replicative stress and DNA-dependent protein kinase. *Cell Cycle*, 2010, **9**, 995–1004.
8. Scorah, J. and McGowan, C. H., Claspin and Chk1 regulate replication fork stability by different mechanisms. *Cell Cycle*, 2009, **8**, 1036–1043.
9. Petermann, E., Woodcock, M. and Helleday, T., Chk1 promotes replication fork progression by controlling replication initiation. *Proc. Natl. Acad. Sci. USA*, 2010, **107**, 16090–16105.
10. Bahassi, E. M., Ovesen, J. L., Riesenberg, A. L., Bernstein, W. Z., Hasty, P. E. and Stambrook, P. J., The checkpoint kinases Chk1 and Chk2 regulate the functional associations between hBRCA2 and Rad51 in response to DNA damage. *Oncogene*, 2008, **27**, 3977–3985.
11. Davies, K. D. *et al.*, Single-agent inhibition of Chk1 is antiproliferative in human cancer cell lines *in vitro* and inhibits tumor xenograft growth *in vivo*. *Oncol Res.*, 2011, **19**, 349–363.
12. Cole, K. A. *et al.*, RNAi screen of the protein kinome identifies checkpoint kinase 1 (CHK1) as a therapeutic target in neuroblastoma. *Proc. Natl. Acad. Sci. USA*, 2011, **108**, 3336–3341.
13. Dai, Y. and Grant, S., New insights into checkpoint kinase 1 in the DNA damage response signaling network. *Clin. Cancer Res.*, 2010, **16**, 376–383.
14. Zabludoff, S. D. *et al.*, AZD7762, a novel checkpoint kinase inhibitor, drives checkpoint abrogation and potentiates DNA-targeted therapies. *Mol. Cancer Ther.*, 2008, **9**, 2955–2966.
15. Ashwell, S., Janetka, J. W. and Zabludoff, S., Keeping checkpoint kinases in line: new selective inhibitors in clinical trials. *Expert Opin. Invest. Drugs*, 2008, **17**, 1331–1340.
16. Daud, A. *et al.*, A phase I dose-escalation study of SCH 900776, a selective inhibitor of checkpoint kinase 1 (CHK1), in combination with gemcitabine (Gem) in subjects with advanced solid tumors. *J. Clin. Oncol.*, 2010, **28**, abstract number 3064.
17. Hong, P.-C., *et al.*, Synthesis of selenophene derivatives as novel CHK1 inhibitors. *Bioorg. Med. Chem. Lett.*, 2010, **20**, 5065–5068.
18. Kolossvary, I. and Guida, W. C., Low mode search: an efficient, automated computational method for conformational analysis application to cyclic and acyclic alkanes and cyclic peptides. *J. Am. Chem. Soc.*, 1996, **118**, 5011–5019.
19. Sherman, W., Day, T., Jacobson, M. P., Friesner, R. A. and Farid, R., Novel procedure for modeling ligand/receptor induced fit effects. *J. Med. Chem.*, 2006, **49**, 534–553.
20. Sherman, W., Beard, H. S. and Farid, R., Use of an induced fit receptor structure in virtual screening. *Chem. Biol. Drug Des.*, 2006, **67**, 83–84.
21. Merchant, C. A., Briggs, K. A. and Long, A., *In silico* tools for sharing data and knowledge on toxicity and metabolism: derek for windows, meteor, and vatic. *Toxicol. Mech. Methods*, 2008, **18**, 177–187.

ACKNOWLEDGEMENTS. This work was supported by the Council of Scientific and Industrial Research-Unit for Research and Development of Information Products (CSIR-URDIP), Pune and Jamia Hamdard University, New Delhi.

Received 7 April 2015; revised accepted 11 August 2015

doi: 10.18520/v109/i12/2271-2277